JOURNAL OF
APPLIED
CRYSTALLOGRAPHY

ISSN 1600-5767

Two-step GISAXS characterization of $NiSi_2$ nanoplates and Ni nanocrystals embedded in a silicon wafer covered with a silica thin film

Daniel da Silva Costa,[a]* Guinther Kellermann[a] and Aldo F. Craievich[b]

[a]Department of Physics, Federal University of Paraná, Mailbox 19091, Curitiba, Paraná, CEP 81531-990, Brazil, and [b]Institute of Physics, University of Sao Paulo, CP 66318, CEP 05315-970, São Paulo, Brazil. *Correspondence e-mail: daniel.costa@ufpr.br

Received 20 July 2022
Accepted 15 November 2022

Edited by F. Meilleur, Oak Ridge National Laboratory, USA, and North Carolina State University, USA

Keywords: Ni nanocrystals; grazing-incidence small-angle X-ray scattering; GISAXS; $NiSi_2$ nanoplates; Si wafers; nanopores; thin films; isotropic.

Supporting information: this article has supporting information at journals.iucr.org/j

Here, an experimental grazing-incidence small-angle X-ray scattering (GISAXS) study of the nanostructure of a sample composed of a Si(001) wafer covered by a Ni-doped SiO_2 thin film and thermally treated at high temperature is described. Previous studies indicated that this type of composite contains Ni nanocrystals mainly inside the thin film and $NiSi_2$ nanoplates buried in the Si wafer. To achieve accurate determinations of low-resolution structural parameters of the nanoparticles derived from the experimental results (shape, volume and size), two GISAXS patterns were recorded. The first pattern was produced by the Si wafer covered by a nanoporous Ni-doped SiO_2 thin film and the second pattern was recorded after removal of the SiO_2 thin film by chemical etching. By using the procedure of best fitting of a modeled isotropic GISAXS intensity to a set of 1D GISAXS patterns recorded before thin-film removal, the average radius and radius dispersion of a size polydisperse set of spherical Ni nanocrystals were determined. The GISAXS pattern recorded after removal of the SiO_2 thin film was almost completely due to the scattering intensity produced by oriented $NiSi_2$ nanoplates located inside the Si wafer. By fitting a theoretical function for the X-ray scattering intensity produced by oriented nanoplates to a set of experimental 1D GISAXS patterns, the maximum diameters and average thickness of the hexagonal $NiSi_2$ nanoplates were determined. The GISAXS intensity pattern produced by the sample after thin-film removal is essentially anisotropic (with only a weak isotropic contribution from Ni nanocrystals), thus allowing for precise quantitative determinations of the relevant sizes of the $NiSi_2$ nanoplates.

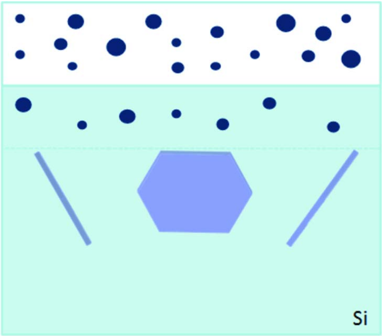

1. Introduction

The search for new methods to prepare $CoSi_2$ and $NiSi_2$ nanocrystals coherently grown in single-crystalline Si wafers has increased during recent decades because of the potential applications of these nanocomposites to several areas of nanotechnology (Cheng *et al.*, 2007; Chung-Yang *et al.*, 2009; Wardle *et al.*, 2005). Owing to their rather high electrical conductivity, Co and Ni silicides can be used as contact materials in electronic devices integrated with Si (Chung-Yang *et al.*, 2009). Several studies have demonstrated the potential of nanostructured composites consisting of $NiSi_2$ nanocrystals embedded in a Si single crystal for applications as a thermoelectric material (Liu *et al.*, 2017) and photovoltaic cells (Sachan *et al.*, 2013).

Methods often used to grow $NiSi_2$ nanocrystals in a Si wafer include the deposition of a metallic Ni film directly on bare silicon and a thermal treatment promoting the diffusion of Ni atoms from the thin film into the Si single crystal. However,

https://doi.org/10.1107/S1600576722010974

depending on the thickness of the Ni film, different intermediate phases of Ni silicides richer in Ni are formed prior to the formation of the desired $NiSi_2$ phase. Other more complex methods, such as high-vacuum electron-beam evaporation, have been used for the formation of $NiSi_2$ nanowires (Chuang & Cheng, 2014).

More recently, in order to grow $NiSi_2$ nanoplates in a thin layer located close to the external surface of a Si wafer, a new method was applied (Costa *et al.*, 2022, 2021). This procedure starts from the deposition of liquid solution precursors of a Ni-doped SiO_2 thin film on a flat Si wafer. This precursor wafer–film composite is then submitted to a thermal treatment during which isolated Ni atoms diffuse through the thin film and aggregate, thus yielding spherical Ni nanocrystals, most of them located inside the thin film. Spherical Ni nanocrystals have also been observed in a corroded layer in a Si wafer close to its external surface. The corroded layer is formed during a chemical etching used for removing the native oxide. Scanning transmission electron microscopy (STEM) images of the sample cross section show that the thin film and the corroded layer both have thicknesses within the 80–90 nm range (Costa *et al.*, 2022). Ni atoms also diffuse across the film–wafer interface, react with Si atoms of the Si wafer and build up a number of thin hexagonal $NiSi_2$ nanoplates parallel to the Si{111} crystallographic planes. Previous STEM studies of these samples showed that the $NiSi_2$ phase is composed of hexagonal thin nanoplates, each of them with their large surfaces parallel to one of the four planes of the Si{111} crystallographic form (Costa *et al.*, 2022, 2021). Using this novel preparation method, crystalline $NiSi_2$ nanoplates are formed without prior formation of other intermediate Ni silicide phases.

Previous studies showing the interesting role of the well defined orientations of nanoplates embedded in Si wafers on the transport properties of these nanostructured materials have been reported for nanocomposite thin films (Takashiri *et al.*, 2018; Chen *et al.*, 2020). Thus, the singular morphological and crystallographic characteristics of $NiSi_2$ nanocomposites in conjunction with well established silicon-based integrated circuit technology make them potential materials for developments of novel thermoelectric devices (Mingo *et al.*, 2009; Uchida *et al.*, 2013, 2016; Guo & Huang, 2015).

In the present work, we studied a sample composed of a Si wafer covered by a nanoporous Ni-doped thin film subjected to an isothermal treatment at 700°C. We studied this material using grazing-incidence small-angle X-ray scattering (GISAXS) because this technique allows for the determination of relevant structural parameters over a large surface area of the Si wafer (1 × 15 mm).

We prepared the sample to be studied by using a method similar to that previously described (Costa *et al.*, 2022, 2021). However, because of the effect of strong isotropic scattering intensity produced by Ni nanocrystals compared with the very weak anisotropic scattering intensity produced by $NiSi_2$ nanoplates, we have this time recorded GISAXS patterns twice, before and after removing the SiO_2 thin film by chemical etching. In this way we achieve independent and more precise characterizations of the relevant structural parameters of the Ni nanocrystals embedded in the SiO_2 thin film and more particularly those of the $NiSi_2$ nanoplates buried in the Si(001) wafer.

2. Materials and methods

2.1. Sample preparation

A Si(001) wafer with a surface area of ~15 × 15 mm was washed in acetone and then embedded in a concentrated solution of HSO_4 acid at 80°C for 15 min to remove any remaining organic contaminants from its surface. We then washed the wafer in deionized water and dried it in ambient atmosphere. In order to remove the native SiO_2 oxide from the Si-wafer surface we immersed it in a solution of HF acid (48%) for 1 min and dried it under N_2 flow. Immediately after, the wet solutions containing the thin-film precursors were deposited on one of the surfaces of the Si(001) wafer (Costa *et al.*, 2022, 2021).

We separately deposited the precursor solutions of the Ni-doped SiO_2 films on the surface of the Si wafer using the spin-coating technique. Initially, we deposited the $(NiNO_3)_2{\cdot}6H_2O$ salt dissolved in isopropyl alcohol directly on the bare surface of the silicon substrate. We deposited a second solution on the previously deposited salt film. This solution containing TEOS (0.5 µl – tetraethyl orthosilicate) and HCl (200 µl) in isopropyl alcohol was kept overnight at room temperature for hydrolysis and condensation reactions, resulting in a wet gel. Using this deposition procedure, we aimed to increase the concentration of Ni atoms close to the silicon surface, thus favoring the diffusion of Ni atoms into the Si wafer (Costa *et al.*, 2022, 2021).

After drying in the air for a few minutes, the sample was annealed for 1 h at 700°C under a 50 sccm (standard cubic centimetres per minute) flow rate of H_2 at low pressure (1.2×10^3 Pa) for chemical reduction of Ni in the thin film. This thermal treatment promotes the diffusion of Ni atoms through the thin film and from the thin film into the silicon wafer. As demonstrated in previous work (Costa *et al.*, 2022, 2021), after diffusion into the Si wafer, Ni atoms react with the Si atoms, thus leading to the formation of isolated Ni silicide nanoplates.

2.2. Experimental technique

For the characterization of the nanostructures embedded in the SiO_2 thin film and formed inside the Si wafer, we have used the GISAXS technique. The GISAXS intensity patterns were recorded *ex situ* twice, before and after removing the Ni-doped SiO_2 thin film by chemical etching, immerging the sample for 4 s in HF acid (48%).

GISAXS experiments were performed using a Discover D8 diffractometer from Bruker, equipped with an X-ray micro-source with a Cu target (X-ray wavelength λ = 1.5406 Å) together with a Montel multilayer focalization system and a Vantec 500 2D X-ray detector. To avoid absorption and scattering by air, a vacuum path chamber was placed between the sample and the detector. The sample-to-detector distance was set equal to 333.2 mm.

The incidence angle of the primary X-ray beam at the sample surface (α_i) was selected to be equal to 0.28° for all GISAXS measurements. The critical angle of X-ray total reflection of the SiO_2 thin film – determined from X-ray reflectivity (XRR) measurements – was equal to 0.19°, in agreement with previous results (Costa *et al.*, 2022). This angle is much smaller than the critical angle for bulk SiO_2, thus indicating that the thin film is highly porous with a pore-volume fraction equal to 0.14. From the available data, we calculated the depth for which the intensity of the probing beam I_o decreases down to I_o/e. We found that before removing the thin film the penetration depth was *ca* 300 nm. This penetration length is much higher than the width of the surface layer (~180 nm) in which the $NiSi_2$ nanoplates are located. Therefore, we concluded that the angle of the incident X-ray beam was large enough to probe the Ni nanoparticles embedded in the silica thin film as well as the $NiSi_2$ nanoplates buried in the Si wafer. The X-ray intensity versus depth profile was calculated using the procedure described by Costa *et al.* (2022).

The GISAXS intensity was measured as a function of scattering vector defined as

$$\mathbf{q} = \frac{2\pi}{\lambda} \begin{pmatrix} \cos\alpha_f \cos 2\theta_f - \cos\alpha_i \\ \cos\alpha_f \sin 2\theta_f \\ \sin\alpha_f + \sin\alpha_i \end{pmatrix}, \tag{1}$$

in which λ is the X-ray wavelength, α_i is the incidence angle of the primary X-ray beam on the sample surface, α_f is the angle between the direction of a given scattered beam and the sample surface, and $2\theta_f$ is the angle between the projections of the scattered and incident X-ray beams on the sample surface. We determined the parasitic scattering intensity produced by windows, slits and air gaps between sample and vacuum paths by recording the GISAXS intensity for a flat and homogeneous silicon wafer. The parasitic scattering intensity was then subtracted from the total GISAXS intensity produced by the studied samples.

The thin Si(001) wafer was properly cleaved to obtain (15 × 15 mm) square samples. After cleavage, all sample edges were parallel to Si{110} crystallographic directions. For conducting GISAXS measurements, we placed the square Si(001) wafer covered by the SiO_2 thin film on a flat support and set a grazing-incidence angle of $\alpha_i = 0.28°$. One of the wafer edges, [110], was kept approximately parallel to the direction of the incident beam projected on the surface of the wafer. Under these conditions and considering that each thin $NiSi_2$ nanoplate is parallel to one of the four Si{111} crystallographic planes, we expect that the two streaks of GISAXS intensity along the $[1\bar{1}1]$ and $[\bar{1}11]$ directions should be properly recorded by the 2D X-ray detector.

3. Experimental results

3.1. General features

The recorded GISAXS patterns produced by the Si wafer before and after removal of the SiO_2 thin film are displayed in Figs. 1(*a*) and 1(*b*), respectively. These patterns correspond to 200 min of exposure time. Fig. 1(*a*) exhibits an essentially isotropic scattering intensity with a very weak streak in the left side and Fig. 1(*b*) shows a much weaker isotropic scattering intensity and two prominent straight streaks both making an angle equal to 54.7° with the direction [001]. The directions of the streaks at the left and at the right are Si$[1\bar{1}1]$ and Si$[\bar{1}11]$, respectively, thus confirming that the large surfaces of the $NiSi_2$ nanoplates are parallel to planes of the Si{111} crystallographic form. The other straight streaks corresponding to the nanoplates parallel to Si(111) and Si$(11\bar{1})$ can be recorded by the X-ray detector after rotating the sample 90° around the Si[001] axis.

3.2. 2D GISAXS patterns from the wafer–film composite before film removal

Fig. 1(*a*) shows the 2D GISAXS intensity pattern produced by a Ni-doped SiO_2 thin film on a silicon wafer annealed at

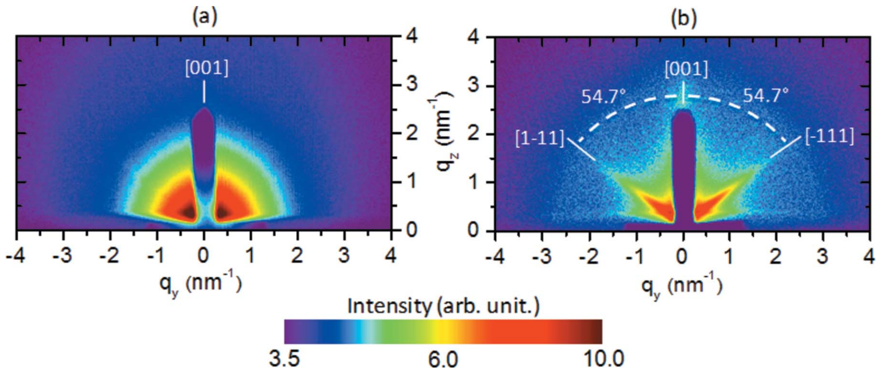

Figure 1
2D GISAXS intensity patterns associated with a Si(001) wafer covered by a Ni-doped SiO_2 thin film after formation of Ni nanocrystals and $NiSi_2$ nanoplates. (*a*) Before removal of the SiO_2 thin film, showing an essentially isotropic scattering intensity. (*b*) After removal of the SiO_2 thin film, showing the presence of an anisotropic contribution to GISAXS intensity, seen as two narrow streaks along the indicated crystallographic directions of the Si(001) wafer. The vertical dark strips in the central part of the patterns are the shadow of the primary beam stopper used for absorbing the primary and reflected X-ray beams.

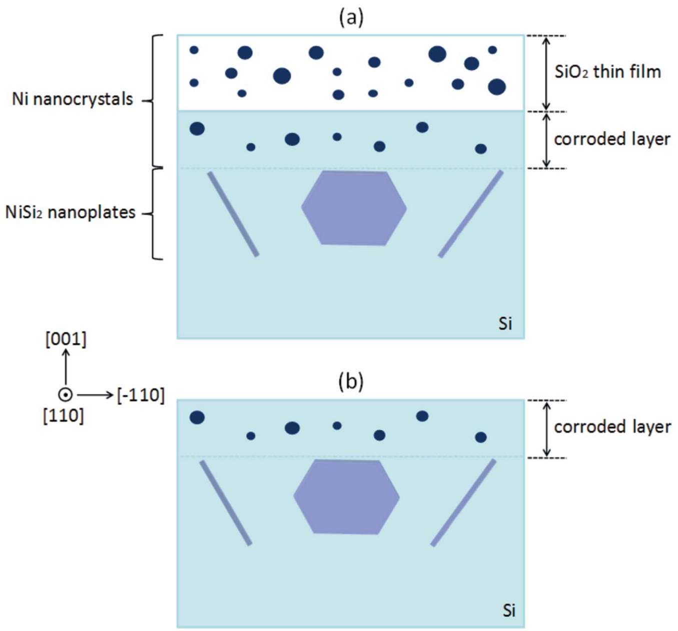

Figure 2
Schematic pictures of the layered structures containing Ni nanocrystals and $NiSi_2$ nanoplates used for modeling the GISAXS intensity by applying equation (2). (*a*) A Si wafer covered by a SiO_2 thin film and (*b*) the same sample after removal of the thin film. The relevant crystallographic directions related to the Si(001) wafer and the locations of the layers containing Ni nanocrystals and $NiSi_2$ nanoplates are indicated.

700°C for 1 h before chemical etching. We note the strong isotropic scattering, which was also observed in previous studies of similar samples prepared under similar conditions (Costa *et al.*, 2022, 2021). Previous STEM studies of similar samples demonstrated the presence of Ni nanocrystals embedded in the SiO_2 thin film and in a corroded layer located inside and close to the surface of the silicon wafer (Costa *et al.*, 2022, 2021). A schematic picture indicating the locations of the Ni nanocrystals in the wafer/thin film composites is shown in Fig. 2.

The observed corroded layer, ~80 nm thick, is located inside and close to the external surface of the Si wafer, as can be seen in Fig. 2. The formation of this corroded layer was attributed to secondary effects of the HF etching used to remove the native oxide from the Si wafer. Removal of the native oxide was expected to favor the diffusion of Ni atoms from the thin film into the Si wafer.

The GISAXS studies also indicated the presence of very small pores inside the SiO_2 film (Costa *et al.*, 2022, 2021). The presence of small pores of a few ångstroms is in fact expected for SiO_2 dry thin films prepared using the sol-gel method (Kesmez *et al.*, 2011; Buckley & Greenblatt, 1994; Li *et al.*, 2004; Sakka, 1989; Silva & Vasconcelos, 1999). In order to account for the contribution from these pores to the total GISAXS intensity, we assumed that they have spherical shape.

Therefore, in line with previous GISAXS studies, we assigned the strong isotropic scattering intensity observed in Fig. 1(*a*) to the presence of Ni nanocrystals embedded in the Ni-doped SiO_2 thin film and in the corroded Si layer, and nanopores inside the SiO_2 film (Costa *et al.*, 2022, 2021). Superposed on the isotropic scattering intensity observed in Fig. 1(*a*), we also note some anisotropic scattering intensity, shown as a weak streak at the left of the pattern.

3.3. 2D GISAXS pattern from the Si wafer after thin-film removal

Fig. 1(*b*) displays the essentially anisotropic GISAXS intensity pattern produced by the studied sample after removal of the Ni-doped SiO_2 thin film by chemical etching. As expected, the isotropic scattering intensity seen in Fig. 1(*a*) is strongly reduced in the pattern shown in Fig. 1(*b*). On the other hand, the anisotropic contribution to the scattering intensity is clearly apparent in Fig. 1(*b*) as nearly symmetrical straight streaks on both sides of the scattering pattern. The observed differences between the GISAXS patterns recorded before and after removal of the SiO_2 thin film confirm the results of previous STEM studies (Costa *et al.*, 2022), which indicated that Ni nanocrystals and nanopores – responsible for most of the contribution of the isotropic scattering intensity – are mainly formed inside the Ni-doped SiO_2 thin film.

The anisotropic GISAXS intensity pattern shown in Fig. 1(*b*) is produced by $NiSi_2$ nanoplates buried in the Si wafer close to but not in contact with the external surface of the Si wafer, as can schematically be seen in Fig. 2(*b*). The anisotropic features of the GISAXS pattern are similar to those observed in previous studies, in which this scattering intensity was attributed to well oriented $NiSi_2$ (Costa *et al.*, 2022, 2021) and $CoSi_2$ (Kellermann *et al.*, 2012, 2015; Costa *et al.*, 2015) nanoplates endotaxially grown in Si(001) wafers. Previous studies (Costa *et al.*, 2022; Kellermann *et al.*, 2012, 2015) demonstrated the presence of $NiSi_2$ and $CoSi_2$ thin nanoplates with nearly hexagonal shape and with their large surfaces parallel to planes of the Si{111} crystallographic form. This implies that the angle between the direction normal to the Si(001) wafer surface and the directions of both streaks should be equal to 54.7°, which is experimentally confirmed for the sample studied in this work, as shown in Fig. 1(*b*).

4. Modeling of GISAXS intensity

As described in the preceding section, the total GISAXS intensity is defined as the sum of the scattering intensities due to (*a*) a polydisperse set of uncorrelated Ni nanocrystals embedded in the SiO_2 thin film and inside a corroded layer close to the surface of the Si wafer, (*b*) a polydisperse set of nanopores with nearly spherical shape embedded in the SiO_2 thin film, and (*c*) a set of well oriented $NiSi_2$ hexagonal nanoplates embedded in the Si wafer. The locations of the Ni nanocrystals and $NiSi_2$ nanoplates are schematically shown in Fig. 2.

Under the above-mentioned assumptions the total GISAXS intensity is given by

$$
\begin{aligned}
I(q) \propto & \left|T(\alpha_{\rm i})\right|^2 \left|T(\alpha_{\rm f})\right|^2 \\
& \times \left\{ \left[c\,\frac{\left(\rho_{\rm Ni} - \rho_{\rm SiO_2}\right)^2}{A_1\left(\tilde{q}_z\right)} + (1-c)\,\frac{\left(\rho_{\rm Ni} - \rho_{\rm Si}\right)^2}{A_2\left(\tilde{q}_z\right)} \right] \right. \\
& \times \int\limits_{R=0}^{\infty} \left(\frac{4}{3}\pi R^3\right)^2 \left|F_{\rm sph}\left(q_\parallel, \tilde{q}_z, R\right)\right|^2 N_{\rm Ni}(R)\,{\rm d}R \\
& + \frac{\left(\rho_{\rm SiO_2}\right)^2}{A_1(\tilde{q}_z)} \int\limits_{R=0}^{\infty} \left(\frac{4}{3}\pi R^3\right)^2 \left|F_{\rm sph}\left(q_\parallel, \tilde{q}_z, R\right)\right|^2 N_{\rm pores}(R)\,{\rm d}R \\
& + \frac{1}{4}\,\frac{\left(\rho_{\rm NiSi_2} - \rho_{\rm Si}\right)^2}{A_3(\tilde{q}_z)} \\
& \left. \times \int\limits_{t=0}^{\infty} \sum_{i=1}^{4} \left|H_i\left(\alpha, \phi, q_\parallel, \tilde{q}_z, D, t\right)\right|^2 N_{\rm H}(t)\,{\rm d}t \right\}, \qquad (2)
\end{aligned}
$$

where $|T(\alpha_{\rm i})|^2$ and $|T(\alpha_{\rm f})|^2$ are the Fresnel transmission functions accounting for the intensity of the refracted and scattered beams at the air/SiO$_2$ and SiO$_2$/Si interfaces; $\alpha_{\rm i}$ and $\alpha_{\rm f}$ are the grazing-incidence angles of the primary and scattered beams, respectively; c is the fraction of Ni nanoparticles in the SiO$_2$ thin film; $\rho_{\rm Ni}$, $\rho_{\rm SiO_2}$, $\rho_{\rm NiSi_2}$ and $\rho_{\rm Si}$ are the electron densities of the Ni nanospheres, SiO$_2$ thin film, NiSi$_2$ nanoplates and silicon wafer, respectively; A_1, A_2 and A_3 are the attenuation factors of the scattering intensity of the Ni nanocrystals, pores and NiSi$_2$ nanoplates, located in the thin film, in the corroded layer at the surface of the Si wafer and in a thin layer in the Si wafer below the corroded layer, respectively; $F_{\rm sph}(R)$ is the scattering amplitude of a sphere with radius R; $N_{\rm Ni}(R)$ and $N_{\rm pores}(R)$ are the radius density distribution functions of the Ni nanoparticles and pores, respectively; H_i is a function describing the scattering amplitude due to a hexagonal silicide nanoplate with maximum diameter D and thickness t; and $N_{\rm H}(t)\,{\rm d}t$ is the number of nanoplates with thickness between t and $t + {\rm d}t$. Since the width of the intensity profiles along the direction parallel to the surface of the nanoplates – related to the maximum diameter D – is very small, the accuracy of the calculated value of the dispersion in D is very poor. For this reason, we did not determine the dispersion in the maximum diameter D. On the other hand, previous results showed a good agreement of the average value $\langle D \rangle$ obtained from STEM images and that determined from GISAXS patterns assuming that nanoplates are monodisperse in diameter (Costa *et al.*, 2022). The index i (from 1 to 4) refers to the four orientations of the nanoplates – which are assumed to be all equally probable – corresponding to the large surfaces of the nanoplates parallel to one of the four possible planes of the Si{111} crystallographic form, as shown in previous work (Costa *et al.*, 2022). Furthermore, α is the angle between the direction normal to the sample surface and the crystallographic Si[001] direction, $\tilde{q}_z$ is the component of the scattering vector normal to the sample surface, ϕ is the azimuthal angle, and $q_\parallel = (q_x^2 + q_y^2)^{1/2}$.

The scattering amplitudes associated with spheres, $F_{\rm sph}(R)$, and hexagonal nanoplates, $H_i(\alpha, \phi, q_\parallel, \tilde{q}_z, D, t)$, with one of their lateral sides parallel to the Si(001) planes and with their large surfaces forming a 54.7° angle with the Si(001) direction, together with a detailed discussion describing how interface refraction and reflection effects were accounted for in our analyses, are given in the supplementary material section of a previous article (Costa *et al.*, 2022). The radius distribution functions of Ni nanocrystals and nanopores were assumed to be well described by lognormal functions and the nanoplate thickness distribution by a Gaussian function.

Since the procedure of alignment of the incident X-ray beam with an edge of the square wafer was not very precise, the azimuthal angle ϕ was considered as a free parameter for the fitting of the modeled function to the experimental GISAXS results.

5. Quantitative analysis of experimental results

5.1. GISAXS results and fitting of the modeled function

The experimental results from the GISAXS measurements are plotted by symbols in Figs. 3(*a*) and 3(*b*). Fig. 3(*a*) displays a set of experimental GISAXS 1D profiles $I(q_y)$ for several q_z values corresponding to the Si(001) wafer covered by the deposited SiO$_2$ thin film before thin-film removal, and Fig. 3(*b*) shows another set of experimental GISAXS curves produced by the same Si(001) sample from which the SiO$_2$ thin film was previously removed.

The good agreement of the fitted $I(q_y)$ curves with the experimental GISAXS intensity profiles for the several q_zs – as shown in Fig. 3 – provides strong evidence of the accuracy of size and orientation parameters for the NiSi$_2$ nanoplates determined from the experimental patterns. Note that in Fig. 3 the $I(q_y)$ curves corresponding to different q_z values were fitted simultaneously using, for all of them, the same values of the structural parameters: namely, the diameter and thickness of the NiSi$_2$ nanoplates and the average radius and radius dispersion of the Ni nanocrystals.

The continuous lines in Figs. 3(*a*) and 3(*b*) are the 1D GISAXS intensity functions, $I(q_y)$, defined by equation (2), that best fit the 1D experimental curves corresponding to several scattering wavenumbers, ranging from $q_z = 0.572$ nm^{-1} up to $q_z = 0.975$ nm^{-1}. The fitting parameters were the number (in relative units), average maximum diameter, average thickness and dispersion in thickness of the NiSi$_2$ nanoplates; and the number (in relative units), average radius and radius dispersion of the Ni nanocrystals. As will be shown in the next sections, we determined the average radius of the spherical Ni nanocrystals, as well as the average diameter, thickness and dispersion in thickness of the NiSi$_2$ nanoplates, by simultaneous fittings of equation (2) to all $I(q_y)$ profiles.

A set of GISAXS intensity curves showing the contribution of each type of scattering object (Ni nanocrystals, nanopores and NiSi$_2$ nanoplates), corresponding to the different terms of equation (2), is given in the supplementary material of Costa *et al.* (2022). The values of the fitting procedure are summarized in Table 1. Details of the determination of the fitting

Table 1
The size parameters derived from the fitting procedure: average radius $\langle R\rangle$ and radius dispersion σ_R of the Ni nanocrystals, and average thickness $\langle t\rangle$, thickness dispersion σ_t and average maximum diameter $\langle D\rangle$ of the $NiSi_2$ nanoplates.

Ni nanocrystals	$\langle R\rangle$ (nm)	2.7 ± 0.5
	σ_R (nm)	0.50 ± 0.05
$NiSi_2$ nanoplates	$\langle t\rangle$ (nm)	8.5 ± 0.4
	σ_t (nm)	4.0 ± 0.8
	$\langle D\rangle$ (nm)	60 ± 3

parameters and associated features for spherical Ni nanocrystals and hexagonal $NiSi_2$ nanoplates are described in Sections 5.2 and 5.3, respectively.

5.2. GISAXS intensity from Ni nanocrystals and nanopores

The sets of curves shown in Fig. 3(*a*) correspond to the GISAXS intensity produced by spherical Ni nanocrystals embedded in the SiO_2 thin film and in the corroded Si layer and by nanopores embedded in the SiO_2 thin film. The best fitting of equation (2) applied to the set of experimental 1D GISAXS curves displayed in Fig. 3(*a*) indicated the presence of two populations of spherical nano-objects: (i) nanometric Ni crystals located inside the SiO_2 thin film and in the corroded layer of the Si wafer, and (ii) smaller nanopores embedded in the thin film. The presence of Ni nanocrystals inside the thin film and in the corroded layer was previously confirmed by STEM imaging of similar samples (Costa *et al.*, 2022).

From our analysis through best fitting of equation (2) to the 1D GISAXS curves displayed in Fig. 3(*a*), we have shown that the spherical Ni nanocrystals exhibit a rather wide radius distribution, with an average radius $\langle R\rangle$ = (2.7 ± 0.5) nm and radius dispersion σ_R = (0.50 ± 0.05) nm. The size parameters of the spherical Ni nanocrystals are summarized in Table 1.

Fig. 4 displays the volume-weighted radius distribution $V(R) = 4\pi R^3 N_{Ni}/3$ of Ni nanocrystals that we obtained from the analysis of the GISAXS patterns recorded before (blue line) and after (red line) removal of the SiO_2 thin film. The features of the curve in red in Fig. 4 indicate that, after etching, only a small fraction of spherical nanoparticles remains inside the Si wafer. This can be explained by the fact that the HF acid is efficient in dissolving the SiO_2 but it cannot break Si—Si bindings. Therefore, the remaining Ni nanoparticles are expected to be formed inside the corroded layer near the surface of the Si wafer, which is less affected by HF etching. Previous analyses by STEM showed the presence of Ni nanocrystals inside the corroded layer of the Si wafer (Costa *et al.*, 2022).

In order to achieve a good fitting of the curves modeled by equation (2) and corresponding to the isotropic GISAXS intensity, we have included a minor contribution from nano-objects much smaller than the Ni nanocrystals. Together with the scattering intensity produced by Ni nanocrystals and $NiSi_2$ nanoplates, we also observed a very broad contribution to GISAXS intensity produced by very small scattering objects (with radii of <1 nm). We have assigned this minor contribution to the presence of nanopores embedded in the thin film. On the other hand, the presence of a rather high nanoporosity

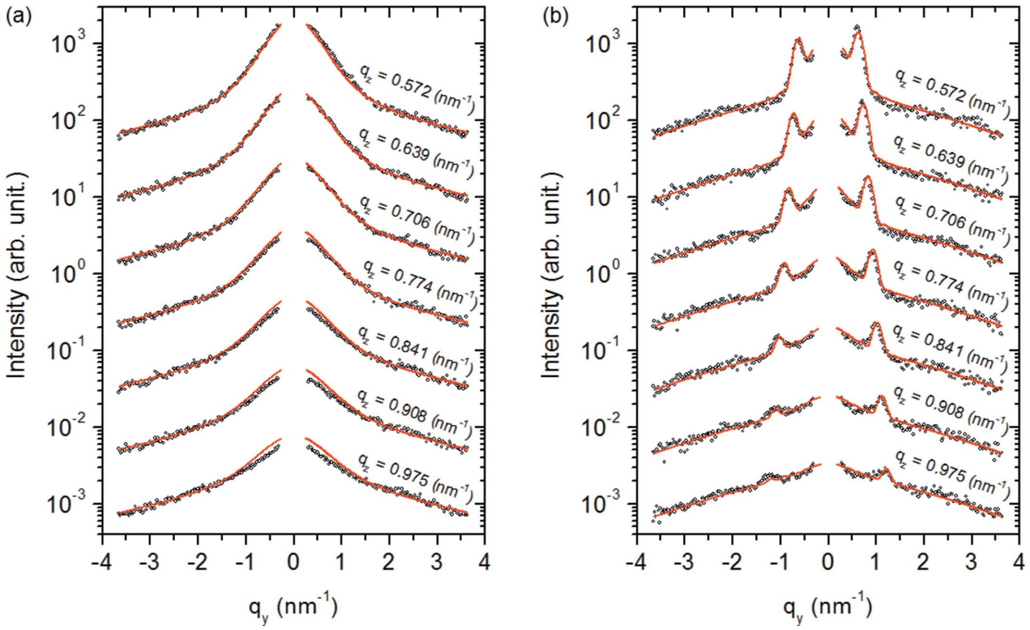

Figure 3
Sets of 1D GISAXS intensity profiles $I(q_y)$, for different q_z values. The symbols denote the experimental results and the red solid lines are the calculated curves corresponding to the best fits of equation (2) to all the experimental 1D scattering profiles. The azimuthal angle for the best-fitted function was determined to be $\phi = 0.85°$. (*a*) 1D GISAXS curves extracted from the pattern shown in Fig. 1(*a*) corresponding to the sample before removal of the Ni-doped SiO_2 thin film. This scattering intensity is essentially isotropic and produced by spherical Ni nanocrystals embedded in the SiO_2 film and inside the corroded Si layer. (*b*) 1D GISAXS profiles extracted from the pattern shown in Fig. 1(*b*) corresponding to the same sample after removal of the thin film. The peaks that are apparent in all the 1D GISAXS curves displayed in (*b*) are related to the straight streaks shown in Fig. 1(*b*).

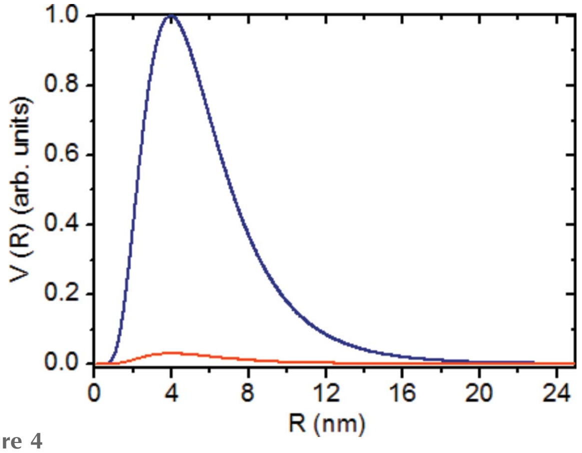

Figure 4
The volume-weighted radius distribution function $V(R) = 4\pi R^3 N_{\rm Ni}/3$ derived from GISAXS results corresponding to Ni nanospheres before (blue) and after (red) removal of the SiO_2 thin film.

in the silica thin film was confirmed by our XRR measurements, as previously described in Section 2.2. The determination of the average size of these pores would require GISAXS measurements over a q range much larger than that accessible by our experimental setup. For this reason, we did not perform any further analysis of the GISAXS intensity produced by nanopores.

5.3. GISAXS intensity from $NiSi_2$ nanoplates

The curves displayed in Fig. 3(*b*) are essentially produced by the hexagonal $NiSi_2$ nanoplates buried in a thin layer in the Si wafer, as shown in Fig. 2. In Fig. 3(*b*) there is a weak asymmetry with respect to $q_y = 0$ in the GISAXS intensity produced by the $NiSi_2$ nanoplates. This anisotropy is *a priori* expected for the present experimental conditions, *i.e.* an azimuthal angle different from zero ($\phi = 0.85^\circ$) and an incidence angle obviously different from zero ($\alpha_{\rm i} = 0.28^\circ$).

The average maximum diameter and thickness of the hexagonal $NiSi_2$ nanoplates determined from the best fitting of equation (2) to the experimental 1D GISAXS curves displayed in Fig. 3(*b*) are $\langle D\rangle = (60 \pm 3)$ nm and $\langle t\rangle = (8.5 \pm 0.4)$ nm, respectively, and the dispersion in thickness is $\sigma_t = (4.0 \pm 0.8)$ nm. The size parameters of the $NiSi_2$ nanoplates are summarized in Table 1.

The values of $\langle D\rangle$ and $\langle t\rangle$ are smaller than those determined in previous studies, in which samples were obtained under different preparation conditions (Costa *et al.*, 2022, 2021). The sample studied here was heat treated at 700°C under a 50 sccm H_2 flow rate, while in previous studies the samples were heat treated at lower temperatures, namely 500°C (Costa *et al.*, 2022) and 405°C (Costa *et al.*, 2021), under a H_2 flow rate four times larger.

Additional 2D GISAXS patterns for different azimuthal angles ϕ ranging from -8.15° up to 9.85° are shown in the supporting information (Fig. S1) together with the simulated intensity patterns calculated using the fitting parameters determined from the pattern shown in Fig. 1(*b*). A visual comparison indicates that all the experimental patterns agree well with the simulated patterns for the different azimuthal angles, thus demonstrating the good quality of the modeled GISAXS function and the consistency of the fitting procedure.

6. Conclusions

In this work we have studied, using a two-step GISAXS procedure, the nanostructural features of a Si(001) wafer covered by a Ni-doped SiO_2 thin film after being submitted to an isothermal treatment at 700°C under H_2 atmosphere. We have recorded two 2D GISAXS patterns, one of them before and another after removal of the SiO_2 thin film by chemical etching. This procedure led to independent determinations of the structural parameters related to the spherical Ni nanocrystals and hexagonal $NiSi_2$ nanoplates grown inside the Si wafer and inside the deposited SiO_2 thin film.

The features of the 2D GISAXS intensity pattern recorded before thin-film removal showed the presence of strong isotropic scattering intensity produced by spherical Ni nanocrystals and small empty nanopores embedded in the SiO_2 thin film, with a very weak contribution from well oriented $NiSi_2$ nanoplates located inside the Si wafer. From our analysis of the isotropic component of the GISAXS intensity through fitting a modeled function to a set of 1D GISAXS $I(q_y)$ curves for different q_z values, we have determined the average radius and radius dispersion of the Ni nanocrystals.

The features of the 2D GISAXS pattern recorded after SiO_2 thin-film removal indicate a predominant contribution to the anisotropic scattering intensity by oriented $NiSi_2$ nanoplates located inside the Si(001) wafer. By simultaneous fittings of a modeled function to a set of several 1D GISAXS $I(q_y)$ curves for different q_z values, we have determined the maximum diameter and the thickness distribution of the hexagonal $NiSi_2$ nanoplates.

Our results indicate that the quality of the structural information of multilayered materials derived from the analysis of a single GISAXS pattern of multilayered samples can be improved by independently recording and analyzing several GISAXS patterns after successive chemical removals of outer layers. Furthermore, in order to determine size parameters with improved quality from GISAXS data for other similar materials – such as $CoSi_2$ nanoplates buried in a Si wafer covered with a SiO_2 thin film – additional studies applying the same method of SiO_2 thin-film removal are being planned.

Funding information

Conselho Nacional de Desenvolvimento Científico e Tecnológico - CNPq Processo 420781/2016-1 and Pro-Reitoria de Pesquisa e Pós-Graduação – UFPR - Edital 004/2019 – Apoio a Atividades de Pesquisa – CPDCT/PRPPG/UFPR Processo 23075.044816/2019-95.

References

Buckley, A. M. & Greenblatt, M. (1994). *J. Chem. Educ.* **71**, 599–602.

Chen, X., Zhou, Z., Lin, Y. & Nan, C. (2020). *J. Materiomics*, **6**, 494–512.

Cheng, S. L., Lu, S. W., Wong, S. L., Chang, C. C. & Chen, H. (2007). *J. Cryst. Growth*, **300**, 473–477.

Chuang, C. & Cheng, S. (2014). *Nano Res.* **7**, 1592–1603.

Chung-Yang, L., Ming-Pei, L., Kao-Feng, L., Wei-Fan, L., Chi-Te, H., Sheng-Yu, C. & Lih-Juann, C. (2009). *J. Phys. Chem. C*, **113**, 2286–2289.

Costa, D. S., Huck-Iriart, C., Kellermann, G., Giovanetti, L. J., Craievich, A. F. & Requejo, F. G. (2015). *Appl. Phys. Lett.* **107**, 223101.

Costa, D. S., Kellermann, G., Craievich, A. F., Giovanetti, L. J., Huck-Iriart, C. & Requejo, F. G. (2021). *J. Alloys Compd.* **879**, 160345.

Costa, D. S., Kellermann, G., Craievich, A. F., Montoro, L. A., Oliveira, C. K. B. Q. M., Afonso, C. R. M., Huck-Iriart, C., Giovanetti, L. J., Requejo, F. G., Zanella, I. G., Mazzaro, I., Szameitat, E. S. & Cardoso, R. P. (2022). *Surf. Interfaces*, **29**, 101763.

Guo, R. & Huang, B. (2015). *Sci. Rep.* **5**, 9579.

Kellermann, G., Montoro, L. A., Giovanetti, L. J., dos Santos Claro, P. C., Zhang, L., Ramirez, A. J., Requejo, F. G. & Craievich, A. F. (2012). *Appl. Phys. Lett.* **100**, 063116.

Kellermann, G., Montoro, L. A., Giovanetti, L. J., dos Santos Claro, P. C., Zhang, L., Ramirez, A. J., Requejo, F. G. & Craievich, A. F. (2015). *Phys. Chem. Chem. Phys.* **17**, 4945–4951.

Kesmez, O., Burunkaya, E., Kiraz, N., Çamurlu, H. E., Asiltürk, M. & Arpaç, E. (2011). *J. Non-Cryst. Solids*, **357**, 3130–3135.

Li, L., Zhang, L. & Yao, X. (2004). *Ceram. Int.* **30**, 1843–1846.

Liu, W., Hu, J. S., Zhang, S., Deng, M., Han, C.-G. & Liu, Y. (2017). *Mater. Today Phys.* **1**, 50–60.

Mingo, N., Hauser, D., Kobayashi, N. P., Plissonnier, M. & Shakouri, A. (2009). *Nano Lett.* **9**, 711–715.

Sachan, R., Gonzalez, C., Dyck, O., Wu, Y., Garcia, H., Pennycook, S. J., Rack, P. D., Duscher, G. & Kalyanaraman, R. (2013). *Nanomater. Energ.* **2**, 11–19.

Sakka, S. (1989). *Part. J.* **7**, 106–118.

Silva, R. F. & Vasconcelos, W. L. (1999). *Mat. Res.* **2**, 197–200.

Takashiri, M., Hagiwara, K. & Hamada, J. (2018). *Vacuum*, **157**, 216–222.

Uchida, N., Ohishi, Y., Miyazaki, Y., Kurosaki, K., Yamanaka, S. & Tada, T. (2016). *Mater. Trans.* **57**, 1076–1081.

Uchida, N., Tada, T., Ohishi, Y., Miyazaki, Y., Kurosaki, K. & Yamanaka, S. (2013). *J. Appl. Phys.* **114**, 134311.

Wardle, M. G., Goss, J. P., Briddon, P. R. & Jones, R. (2005). *Phys. Status Solidi A*, **202**, 883–888.